R. Feil, T. Pflumm, P. Bortolotti, M. Morandini
A Cross-Sectional Aeroelastic Analysis and Structural Optimization Tool for Slender Composite Structures
Composite Structures, Vol. 253, 2020, 112755 (11 pages)
doi:10.1016/j.compstruct.2020.112755

Composite Structures 253 (2020) 112755

Contents lists available at ScienceDirect

Composite Structures

journal homepage: www.elsevier.com/locate/compstruct

A cross-sectional aeroelastic analysis and structural optimization tool for slender composite structures

Roland Feil [a,*], Tobias Pflumm [b], Pietro Bortolotti [a], Marco Morandini [c]

[a] National Renewable Energy Laboratory, Boulder, Colorado, USA
[b] Technical University of Munich, Germany
[c] Politecnico di Milano, Italy

ARTICLE INFO

Keywords:
SONATA
VABS
ANBA4
Parametric design framework
Composite structures

ABSTRACT

A fully open-source available framework for the parametric cross-sectional analysis and design optimization of slender composite structures, such as helicopter or wind turbine blades, is presented. The framework—Structural Optimization and Aeroelastic Analysis (SONATA)—incorporates two structural solvers, the commercial tool VABS, and the novel open-source code ANBA4. SONATA also parameterizes the design inputs, post-processes and visualizes the results, and generates the structural inputs to a variety of aeroelastic analysis tools. It is linked to the optimization library OpenMDAO. This work presents the methodology and explains the fundamental approaches of SONATA. Structural characteristics were successfully verified for both VABS and ANBA4 using box beam examples from literature, thereby verifying the parametric approach to generating the topology and mesh in a cross section as well as the solver integration. The framework was furthermore exercised by analyzing and evaluating a fully resolved highly flexible wind turbine blade. Computed structural characteristics correlated between VABS and ANBA4, including off-diagonal terms. Stresses, strains, and deformations were recovered from loads derived through coupling with aeroelastic analysis. The framework, therefore, proves effective in accurately analyzing and optimizing slender composite structures on a high-fidelity level that is close to a three-dimensional finite element model.

1. Introduction

Modern rotor blades have complex architectures that are defined by a vast number of design parameters. Investigating their constraints and design drivers requires incorporating multidisciplinary perspectives, including the structural dynamics, aerodynamics, materials sciences, and manufacturability restrictions. Therefore, designing blades for either rotorcraft or wind turbine application can be time consuming and expensive. A design approach that combines the structural dynamics and aerodynamics simultaneously rather than iteratively offers a more systematic development process that results in better blades [1]. Hence, effects from aeroelasticity should be considered in the earliest stages of the design process [2].

State-of-the-art aeroelastic analysis tools, such as CAMRAD II [3], Dymore [4], MBDyn [5], and BeamDyn [6] in FAST [7,8] model the blade-structural dynamics with one-dimensional (1D) beam elements. In comparison to fully resolved three-dimensional (3D) finite element models, this approach simplifies the mathematical formulation and increases the computational efficiency [9]. The slender geometrical characteristics of rotor blades proves the simplification of approximating them as 1D beams as sufficient [10]. However, using 1D beam elements decouples the structural characteristics from a realistic composite-blade definition, manufacturability constraints, and blade structural design parameters. Therefore, occurring issues in the blade design are often not discovered until later, when changes become increasingly expensive and time consuming [11]. These issues can be resolved by keeping a strong connection between the aeroelastic and internal structural design. Although fully resolved 3D finite-element models would be the most accurate approach for modeling modern composite rotor blades, they are often not used until the final design stages [9,12] because of their complexity and computational costs. Different ways to approach modeling 1D beams based on 3D structural designs are required.

In 1983, Giavotto et al. [13] developed a general approach for the characterization of anisotropic beams. It uses the de Saint–Venant's principle to determine the Timoshenko stiffness matrix of a beam cross

* Corresponding author.
E-mail addresses: roland-feil@web.de (R. Feil), tobias.pflumm@tum.de (T. Pflumm), pietro.bortolotti@nrel.gov (P. Bortolotti), marco.morandini@polimi.it (M. Morandini).

https://doi.org/10.1016/j.compstruct.2020.112755
Received 29 June 2020; Accepted 27 July 2020
Available online 1 August 2020
0263-8223/Published by Elsevier Ltd.

section. This approach led to a Fortran code, called either ANBA or HANBA, that has never officially been released. Giavotto et al.'s formulation was adopted by many research groups who developed their own version of the code. Among them, NABSA [14] and BECAS [15,16] are worth mentioning. In 1995, Cesnik and Hodges [17] published the Variational Asymptotic Beam Sectional Analysis (VABS) tool that uses the geometrically exact beam theory [18], based on the variational asymptotic method [19], to accurately determine structural characteristics of a two-dimensional (2D) cross section. Since that time, VABS [14,20,21] has evolved and became a popular tool in rotor blade predesign and multidisciplinary rotor design optimization. Its modeling capabilities have been validated in numerous publications [2,22–24].

A slightly different approach was recently proposed by Morandini and Chierichetti [25]. It led to the Python-based open-source code for ANisotropic Beam Analysis: ANBA version 4.0 (ANBA4). The main difference between ANBA4's approach and both previous ANBA versions and VABS can be found in the kinematic description of the displacement field and in the slightly different theoretical approach. Both ANBA and VABS assume that the displacement of an arbitrary point is given by the sum of a cross section's rigid rotations and translations superposed with the warping field. The new approach of ANBA4 instead gets rid of the unknown and redundant cross-section movement and uses displacement of the points as the only unknown of the problem. It is then possible to compute the polynomial solutions of the elastic problem (the so-called de Saint–Venant's solutions) by resorting to the peculiar mathematical structure of the beam problem; see Section 2.5.2. The same approach was later adopted by different authors, including the work from Han and Bauchau [26].

While characterizing the blade's internal structure with common computer-aided design (CAD) tools is feasible, transferring it to a meshed cross section is challenging in an automated design analysis and optimization approach. Therefore, parametric topology and mesh generators with respective preprocessing and postprocessing, as well as plotting functionalities [27] and a robust platform for software integration [28] are needed. Li [29] presented a parametric mesh generator that, although limited to a fixed number of layers with identical thickness, could efficiently model and mesh a cross-sectional layout. Optimizing ply thickness and fiber orientation was conducted using VABS as the structural solver and DYMORE to determine blade loads. Ghiringhelli et al. [30] coupled a custom parametric mesh generator by using an earlier version of ANBA to maximize the active twist authority of a helicopter blade cross section while accounting for simple structural and aeroelastic constraints. By using a response surface method and genetic optimization algorithm, Lim et al. [31] presented the rotor structural design optimization of a compound rotorcraft by varying the web positions, number of plies, and fiber orientation. The approach included multiple constraints such as structural integrity, location of shear center, and discrete ply orientation. VABS was used as structural solver, and CAMRAD II was used to conduct the aeromechanical analysis.

Supported by the U.S. Army, Rohl et al. [2,11] presented IXGEN, a cross-section mesh generator that uses a graphical modeling interface to define the composite layup of a rotor blade. Cross-sectional features such as webs, spar caps, and wrapping layers can be used as design variables during an optimization. The stiffness properties were determined with VABS and applied to RCAS. IXGEN uses OpenCascade, an open-source CAD geometry kernel to generate 3D blade geometries and 2D cross-sectional meshes. The framework was applied to the aeroelastic analysis and design of an active twist rotor [32,33], resulting in a maximization of the actuator authority. Recently, to design reduced-emission rotorcraft, Silva and Johnson [28] began integrating IXGEN into RCOTools [34], a Python-based interface between various rotorcraft analysis tools, such as CAMRAD II, NDARC, and OpenMDAO. Glaz et al. [35,36] again used VABS, applying a surrogate-based optimization approach to successfully reduce helicopter blade vibrations by optimizing the structural design. Wind-energy-related approaches were mostly derived from the aerospace world, using tools such as VABS or BECAS. Chen et al. [37] assessed multiple solvers for cross-sectional analysis of composite wind turbine blades, concluding that other tools such as PreComp [38], FAROB [39], and CROSTAB [40] perform in an inferior manner compared to VABS.

This work presents the Structural Optimization and Aeroelastic Analysis (SONATA) framework to address the continuing need [31,41,42] for a comprehensive and multidisciplinary structural design analysis and optimization environment. It includes the determination of cross-sectional structural properties and stress and strain recovery, and accounts for design and material constraints. The framework can be applied to design applications for arbitrary slender composite structures, including rotorcraft and wind turbine blades. It incorporates both VABS as the community-approved tool to solve structural properties, and ANBA4 as an additional fully open-source solver. Current focus is on the validation and verification of SONATA capabilities, and presentation of the analysis methodology, including the parametric topology and mesh generation of cross sections, determination of structural characteristics, recovery analysis, and implemented preprocessing and postprocessing functionalities.

In the following, the individual modules and capabilities from SONATA are described and validated using box beam examples from literature. The final analysis and evaluation of a fully resolved wind turbine blade showcases the tool's applicability to complex applications, including recovery analysis bases on loads determined through coupling with aeroelastic analysis. Code-to-code comparison between VABS and ANBA4 further verifies the structural solver modules.

2. Methodology

SONATA closes the gap between 1D beam finite element models and the 3D blade design. The 1D finite element model, which is required for specifying elastic beam models in aeroelastic analysis tools, is characterized by evaluating multiple 2D cross sections of a slender composite structure; see Fig. 1. SONATA incorporates a multidisciplinary rotor-blade design framework; see Fig. 2. Its automatized and parametric setup intends to analyze and optimize slender structures with composite layers being placed in a circumferential uniform scheme, and therefore, antisymmetric configuration. Such layup configurations are commonly applied to modern rotorcraft and wind turbine blades. SONATA comprises five main components: parametrization and surface generation, topology generation, mesh discretization, solving for the structural properties, and evaluating as well as postprocessing of the results. SONATA is based on Python. Its cross-sectional beam model (CBM) uses the CAD-Kernel OpenCASCADE with pythonOCC [43].

3D stress and strain recovery can either be performed by applying user-selected load inputs or determined loads from aeroelastic analysis; see Fig. 2. The latter is especially useful when applied to, and wrapped in, an OpenMDAO [44] optimization. To date, such wrappers have been implemented for Dymore [45,46] and CAMRAD II [34] with application to rotorcraft, and for BeamDyn [6] with application to wind turbines. Existing OpenMDAO structures can fairly easily be adapted to feature other aeroelastic analysis codes. The focus of this work is to present and validate the analysis capabilities; detailed optimization studies will be subject to follow-up publications. The following subsections provide an overview on the fundamental SONATA analysis components, including descriptions of essential conventions and definitions.

2.1. Coordinate systems

The global coordinate system (see Fig. 3) is called the blade frame (superscript B). The radial grid of the investigated composite structure spans along the x_1^B-axis. Directions, x_2^B and x_3^B, then provide the area of

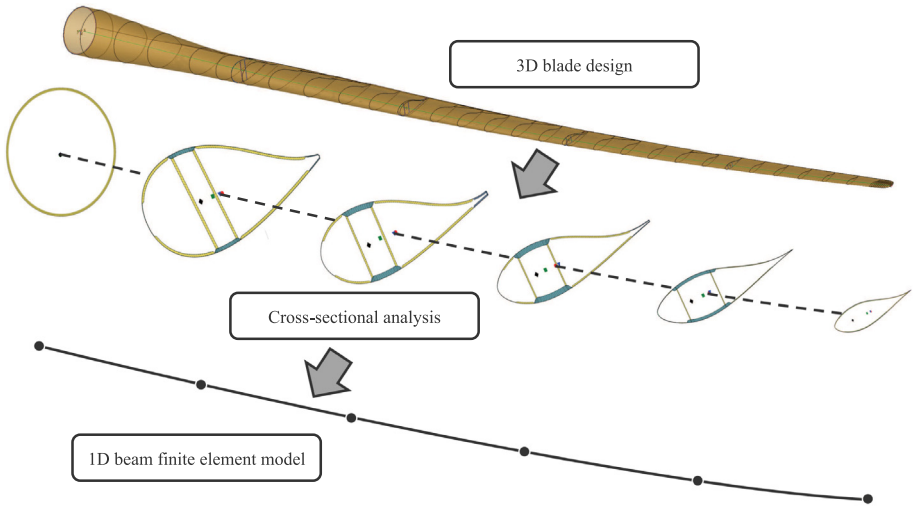

Fig. 1. Methodology to account for 3D structural designs in 1D beam finite element models.

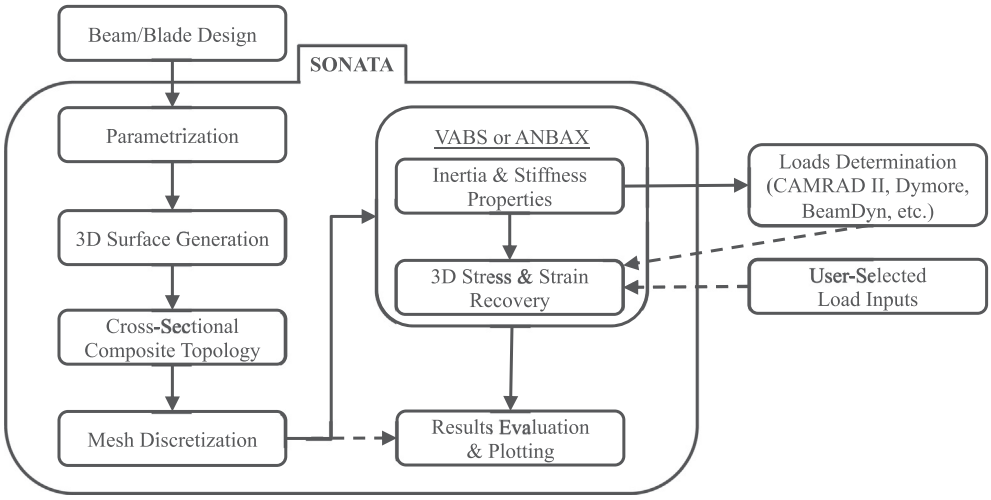

Fig. 2. SONATA analysis procedure.

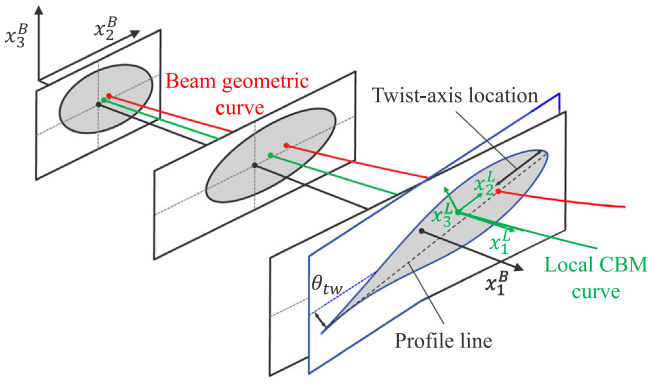

Fig. 3. Illustration of beam definitions.

a cross section at user-defined radial grid locations, or x_1^B-stations, respectively. The outer shape of a beam or blade is defined as wireframes by a collection of airfoils, or other arbitrary outer shapes, which are projected along the nondimensional x_1^B-axis, translated to the nondimensional twist-axis location (scaled to chord length), rotated by the twist angle, Θ_{tw}, around x_1^B, scaled to the desired chord length, and moved onto the beam geometric curve. Because the beam geometric curve arbitrarily bends and twists, the structural mass and stiffness properties are determined in respect to the local coordinate system (superscript L) of the CBM, an independent axes definition that results in the local CBM curve. The unit vector of x_1^L is tangent to the local CBM curve, and the unit vectors of x_2^L and x_3^L are in the plane normal to the local CBM curve, with x_2^L pointing to the leading edge parallel to the chord. This separation allows evaluation of cross-sectional properties at arbitrary reference locations within a cross section, independent from the outer geometry. Assuming the modeling of blade twist and curvature to be part of an aeroelastic analysis model would require the local CBM curve to be identical to the beam geometric curve.

Fig. 4 illustrates the conventions in a 2D cross section. The twist-reference location is on the beam geometric curve, and the L-coordinates lie on the local CBM curve; see Fig. 3. Start and end locations of the elements within the internal structural 2D finite element model are defined using the counter-clockwise s-coordinates; see Fig. 4. Its origin is typically located on the trailing edge.

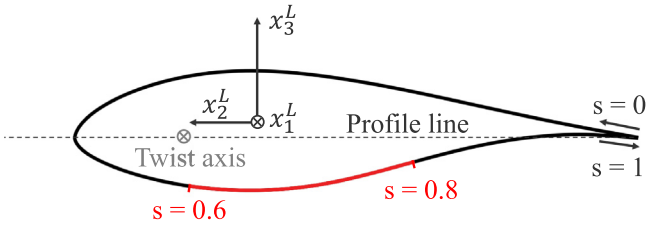

Fig. 4. Local coordinate system (L) and s-coordinates along the arc of an outer shape of a cross section.

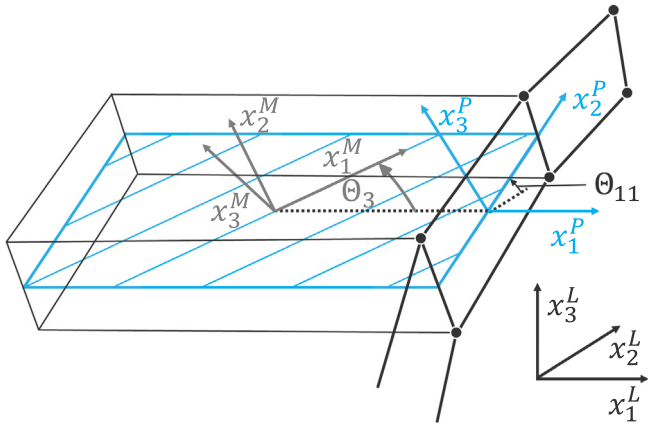

Fig. 5. Plane (P) and material (M) coordinate systems in respect to the local coordinate system (L).

The s-coordinates are nondimensional and range from 0 to 1 along the outer-boundary curve of the airfoil. They propagate through the segments and layers with an interval tree structure as sets of consecutive B-splines. This method allows to efficiently find the intervals of overlapping layers and to locate the corresponding start and end locations of each layer. The material plane defines the orientation of each mesh element rotated by the ply orientation angle, Θ_{11}, around the x_1^L-axis, resulting in the ply-coordinate system, *P*; see Fig. 5. The ply orientation angle is determined automatically in respect to the set of B-splines defining each layer. Finally, the P-frame is rotated around the x_3^P-axis by the given material orientation angle, Θ_3, of an individual layer, resulting in the material-coordinate system, *M*.

2.2. Initialization and parametrization

SONATA input files are defined using the YAML syntax. It provides definitions of the outer shape and orientation in space of the beam or blade, including the twist, chord, twist-reference location, airfoil definitions, and required axis locations along the radial grid. Further inputs are the internal structure of the cross sections, including webs, segments, and layers at arbitrary radial locations, airfoil outer shapes, and a database for material properties. The latter can accommodate isotropic, orthotropic, and anisotropic materials with a respective reference index for identifications. The material orientation angle is neglected for layers with an isotropic material, such as for core material. Once the beam or blade design is loaded, the data are parameterized according to user-defined radial stations.

2.3. Topology

The method for generating the cross-sectional topology was inspired from manufacturing processes, where layers are placed on top of each other in negative molds consecutively from the outside to the inside. Each layer is described by its thickness, start and end locations in regard to the s-coordinates (see Fig. 4), a fiber-orientation angle, and an assigned material. The topology introduces multiple segments that can each include various numbers of layers. The first segment includes the layup attached to the outer-boundary curve of the airfoil. Following segments are ordered subsequently from the leading to the trailing edge and separated by webs attached to the innermost layer of the first segment. Webs are defined as an either straight or curved line between two s-coordinate locations. Fig. 6 shows a generic example of a composite-blade cross section. It demonstrates the topology capabilities of SONATA and accounts for the most common topology requirements from rotorcraft or wind turbine blades, including (from the leading to the trailing edge) shell layers and a c-spar with filled cavities and an added circular trim mass, a box beam, spar caps connected by webs, shell fillers, and trailing edge reinforcements. Each segment can include multiple layers that can be individually associated with different material properties and optional core materials.

The boundary curves separating the segments (i.e., the webs) and each layer within a segment are represented using counterclockwise sets of consecutive B-splines, with the airfoil outer shape being the outermost B-spline. Each layer is generated by performing a parallel offset according to the layer thickness of an existing B-spline and within its start and end positions, which are defined in s-coordinates. Child B-splines are connected to the parent B-splines with added smooth-layer cutoffs at the start and end locations.

2.4. Meshing

Once the cross-sectional topology has been generated, while respecting the layup definitions, the mesh discretization follows in a reverse order, from the inside to the outside. Each layer is meshed by orthogonal projections and corner-style differentiation. Fig. 7 shows the first six cornerstyles that are currently implemented in SONATA. A layer is described by a set of two B-splines, the inner, $a_{B-spline}$, and the outer, $b_{B-spline}$. The nodes on each B-spline are called, accordingly, a_{nodes} and b_{nodes}. First, existing a_{nodes} are determined. In case that nodes are missing on the $a_{B-spline}$, additional uniformly placed nodes are introduced. Then, each node is projected in an orthogonal manner to the $b_{B-spline}$. If multiple projections exist (see Fig. 7), the number of projections (i.e., potential b_{nodes}) and the angle, α, between the range of projections are determined. Next, depending on the pro-

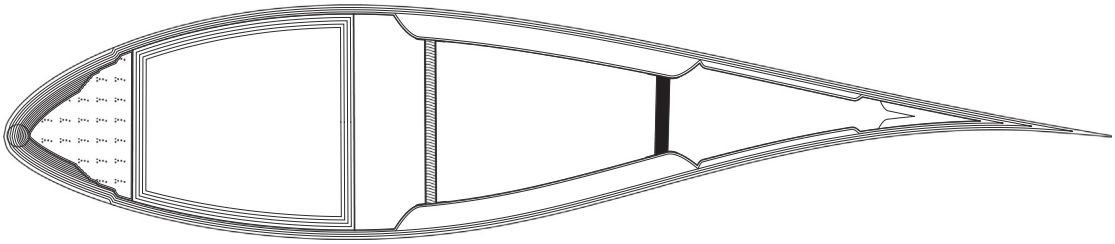

Fig. 6. Topology of a generic composite-blade cross section.

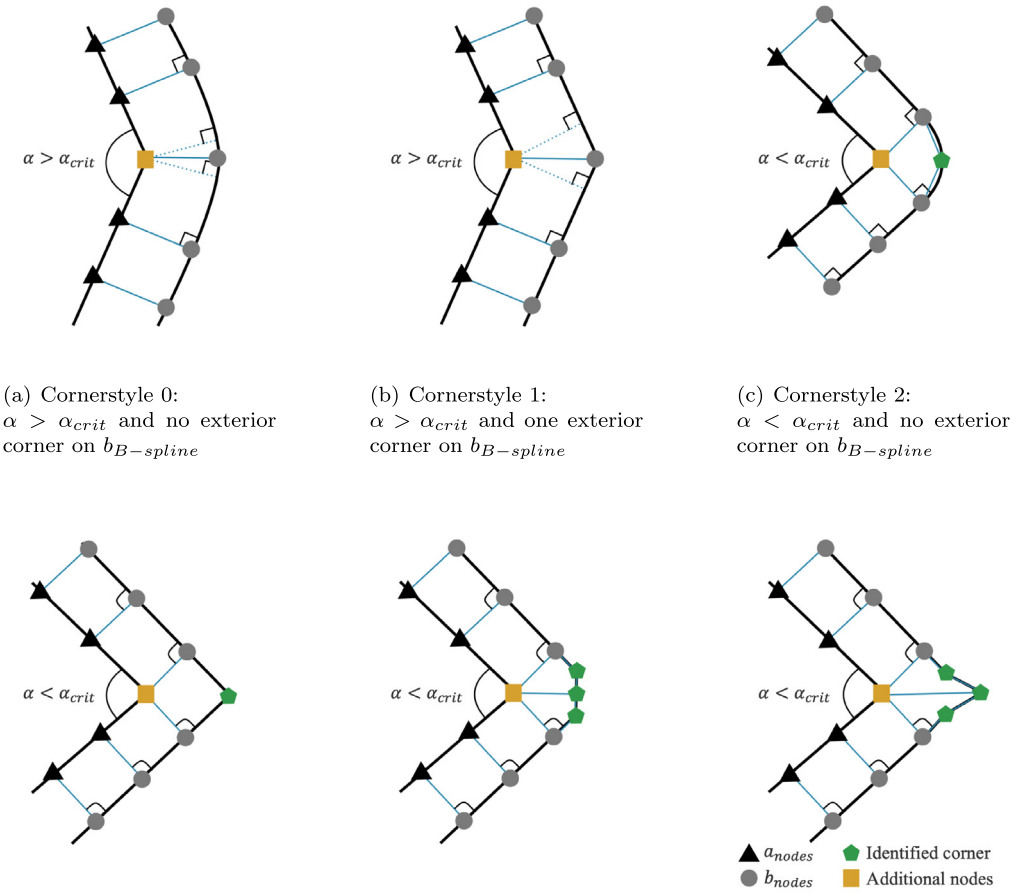

(a) Cornerstyle 0: $\alpha > \alpha_{crit}$ and no exterior corner on $b_{B-spline}$

(b) Cornerstyle 1: $\alpha > \alpha_{crit}$ and one exterior corner on $b_{B-spline}$

(c) Cornerstyle 2: $\alpha < \alpha_{crit}$ and no exterior corner on $b_{B-spline}$

(d) Cornerstyle 3: $\alpha < \alpha_{crit}$ and one exterior corner on $b_{B-spline}$

(e) Cornerstyle 4: $\alpha < \alpha_{crit}$ and two exterior corners on $b_{B-spline}$

(f) Cornerstyle 5: $\alpha < \alpha_{crit}$ and three exterior corners on $b_{B-spline}$

Fig. 7. Cornerstyles 0 to 5 between two sets of B-splines, the inner $a_{B-spline}$ with the a_{nodes}, and the outer $b_{B-spline}$ with the b_{nodes}.

jection angle, α, the defined critical projection angle, α_{crit}, and the number of potential exterior corners in between, the specific cornerstyle and the meshing procedure are determined. After all the nodes are placed on a set of B-splines, they are connected to form cells with associated material properties and fiber-orientation angles. Subsequent steps improve the mesh quality by modifying sharp and large aspect-ratio cells and cell-orientation angles. Once every layer in a segment has been meshed, remaining cavities are triangulated using the Shewchuk [47] algorithm with an area constraint. Hanging nodes between two neighboring segments are avoided by consolidating the cells on the web interfaces.

An optional and final step integrates geometrical shapes in an existing mesh. SONATA currently supports the use of circular trim masses, which can be modified to other arbitrary geometries. The corresponding method to map existing nodes onto the contour line of a specified shape is illustrated in Fig. 8. First, the number of inner nodes for each cell is determined. During step 1, the inner node of each cell marked with 1 (i.e., one node of that cell is inside the shape) is moved along the cell edge with the shortest distance to the intersecting curve. Step 2 then moves remaining inner nodes of cells marked with 2 along the cell edge, again, with the shortest distance to the intersecting curve. Finally, step 3 moves the outer nodes of cells marked with 3 along the edge direction onto the intersecting curve. Once the process is completed, inner cells marked with 3 and 4 are deleted, and a new unstructured mesh is introduced inside the given shape and allocated to a defined material property.

SONATA is further capable of splitting quadrature mesh elements into triangles. This is especially useful for the ANBA4 solver that consistently requires either quadrature or triangular mesh elements, but does not support the combination of those. Fig. 9 shows a completely discretized mesh with triangular elements of a cross section displayed

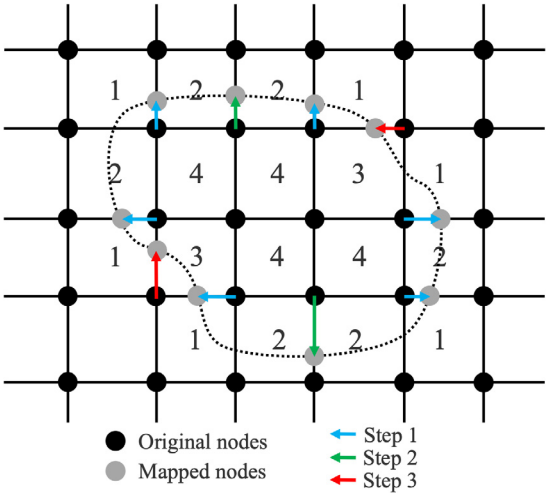

Fig. 8. Mapping algorithm to integrate curves into an existing mesh.

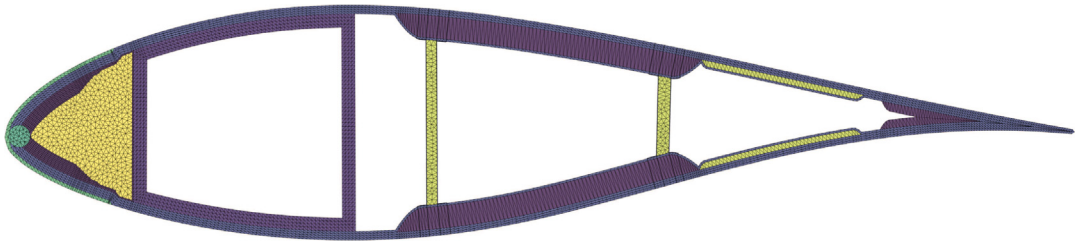

Fig. 9. Mesh discretization of a generic composite-blade cross section.

for a generic composite blade. It is based on the same topology as previously shown in Fig. 6. The final mesh of a cross section along with its associated material properties are then processed and connected to the solver, either VABS or ANBA4.

2.5. Solver

SONATA has been implemented to either use the commercial solver VABS or the open-source solver ANBA4 for conducting the cross-sectional structural analysis at various sections of slender composite structures.

2.5.1. VABS

VABS uses the geometrically exact beam theory [18], based on the variational asymptotic method [19] for determining cross-sectional structural characteristics. The theory behind it has been explained by Hodges [48]; for a more detailed insight, refer to some of the numerous publications with and about VABS [2,14,20–23]. VABS can nowadays be seen as the standard in both industry and academia for conducting cross-sectional analysis of composite structures. Studies in this work were conducted with VABS version 3.4 [21].

2.5.2. ANBA4

At present, ANBA4 (i.e., ANBA version 4.0) is less common compared to VABS. This section, therefore, provides a brief overview of the fundamental mathematics that ANBA4 is based on. More detailed information is given by Morandini et al. [25] as well as Zhu and Morandini [49]. The starting point of ANBA4 is the weak form of the linear equilibrium equations,

$$\int_V \delta\boldsymbol{\varepsilon} : \boldsymbol{\sigma} \mathrm{d}V = \delta\mathcal{L}_e \tag{1}$$

where $\delta\boldsymbol{\varepsilon}$ is the virtual variation of the small strain tensor, $\boldsymbol{\varepsilon} = 1/2(\mathrm{grad}(\boldsymbol{u})^T + \mathrm{grad}(\boldsymbol{u}))$, $\boldsymbol{u}$ is the displacement vector, $\boldsymbol{\sigma} = \mathbb{E} : \boldsymbol{\varepsilon}$ is the Cauchy stress tensor, $\mathbb{E}$ the elastic tensor, and $\delta\mathcal{L}_e$ is the virtual work of the external loads. Assume a prismatic, nontwisted beam to be loaded only by forces per unit of surface, $\boldsymbol{f}$, at its extremities; i.e., the start and end radial stations. Integration by parts along the local CBM curve, x_1^L, of the left-hand side of Eq. (1), leads to

$$\int_L \int_A \delta\boldsymbol{u} \cdot \frac{\partial \boldsymbol{\sigma}_n}{\partial x_1^L} + \delta\mathrm{grad}_S(\boldsymbol{u}) : \boldsymbol{\sigma}_S \mathrm{d}A\mathrm{d}s = \left[\int_A \delta\boldsymbol{u}(\boldsymbol{\sigma}_n - \boldsymbol{f})\mathrm{d}A\right]_L + \left[\int_A \delta\boldsymbol{u}(-\boldsymbol{\sigma}_n - \boldsymbol{f})\mathrm{d}A\right]_0 \tag{2}$$

where $\mathrm{grad}_S(\boldsymbol{u})$ is the gradient over the cross-section plane of $\boldsymbol{u}, \boldsymbol{\sigma}_n = \boldsymbol{\sigma} \cdot \boldsymbol{n}$ is the cross-section stress vector, $\boldsymbol{\sigma}_S = \boldsymbol{\sigma} - \boldsymbol{\sigma} \cdot \boldsymbol{n} \otimes \boldsymbol{n}$ is the stress tensor built with the two in-plane stress vectors, and $\boldsymbol{n}$ follows the x_1^L axis direction. The right-hand side of Eq. (2) states the equivalence of the cross-sectional stress vector and of the applied external loads at the beam extremities. The left-hand side states the equilibrium equations along the beam. Thus, the beam is in equilibrium if

$$\int_A \delta\boldsymbol{u} \cdot \frac{\partial \boldsymbol{\sigma}_n}{\partial x_1^L} + \delta\mathrm{grad}_S(\boldsymbol{u}) : \boldsymbol{\sigma}_S \mathrm{d}A\mathrm{d}s = 0 \tag{3}$$

is satisfied along the beam. The key point behind ANBA4's formulation is to recognize that Eq. (3) has a Hamiltonian structure, which is characterized by 12 independent polynomial solutions along the x_1^L axis, that characterize the unknown displacements field, $\boldsymbol{u}$. The first six are simply the rigid body motions, while the remaining six are the solutions for traction (linear axial displacement relative to x_1^L and constant warping), torsion (linear torsional rotation relative to x_1^L and constant warping), bending in two independent directions (quadratic transverse displacement, linear cross-section rotation, and constant warping), and shear-bending (cubic tranverse displacement, quadratic cross-section rotation, linear and constant warping). The solution procedure is as follows:

- Approximate the unknown displacement field, $\boldsymbol{u}$, with a finite element discretization defined over the cross sections, such that

$$\boldsymbol{u}(x_1^L, x_2^L, x_3^L) = \sum_n N_n(x_2^L, x_3^L)\tilde{\boldsymbol{u}}(x_1^L) \tag{4}$$

  where $N_i(x_2^L, x_3^L)$ are the finite element interpolating functions, and $\tilde{\boldsymbol{u}}(x_1^L)$ are the nodal displacements as a function of x_1^L. This, from a practical point of view, requires defining a mesh over the cross section and to choose the element polynomial interpolating order. SONATA, by default, passes a linear order to ANBA4.
- Assemble the matrices obtained by applying the finite element approximation to Eq. (3). In order to actually compute the integrals, it is necessary to specify the different materials, their constitutive laws, and the material coordinate system; see Fig. 5. Because Eq. (3) involves the first derivative of the normal stress vector, $\partial\boldsymbol{\sigma}_n/\partial x_1^L$, three matrices are obtained, and the discretized version of Eq. (3) is

$$\boldsymbol{M}\frac{\partial^2 \tilde{\boldsymbol{u}}}{\partial x_1^{L^2}} - \boldsymbol{H}\frac{\partial \tilde{\boldsymbol{u}}}{\partial x_1^L} - \boldsymbol{E}\tilde{\boldsymbol{u}} = \boldsymbol{0} \tag{5}$$

  Eq. (5) is a second-order homogeneous differential equation. It is characterized by 12 null eigenvalues and organized into 4 independent Jordan chains. The ensuing polynomial solutions are the rigid body motions and the 6 already-described polynomial deformation modes.
- By knowing the polynomial solution up to order k, with $\tilde{\boldsymbol{u}}(x_1^L) = \sum_{i=0}^{k} \tilde{\boldsymbol{u}}_i x_1^{L^i}$, it is possible to compute the polynomial solution of order $k+1$ by solving the linear system

$$\boldsymbol{E}\tilde{\boldsymbol{u}}_{k+1} = \boldsymbol{M}\tilde{\boldsymbol{u}}_{k-1} - \boldsymbol{H}\tilde{\boldsymbol{u}}_k \tag{6}$$

  Six linear systems need to be solved in order to compute the corresponding polynomial deformation modes.
- Once the polynomial solutions are known, the Timoshenko stiffness matrix can be computed by stating the equivalence of the beam internal virtual work per unit of length of the polynomial solutions and the virtual work from the reaction forces and moments of the beam model.

Because matrix $\boldsymbol{E}$ is four times singular, particular care needs to be taken while solving the linear system of Eq. (6). Its nullspace is known analytically and is equal to the three rigid body motions of the beam and its constant rotation around x_1^L. To solve the system, it is thus necessary to either constrain the nullspace by means of Lagrange multipliers or resort to an iterative solver and continuously deflate the nullspace from the solution. Furthermore, in order to correctly compute the cubic solution, one needs to deflate the traction and torsion of the deformable modes from the two constant-bending parabolic solutions.

The current implementation of ANBA4 [50] leverages Dolfin [51,52], a library of the FEniCS project [53,54]. One needs to specify the mesh, material properties, and orientation angles, according to the convention of Fig. 5 and the polynomial degree of the cross-section finite element approximation. After that, one can compute, with a single function call, the six polynomial solutions, the cross-sectional inertia, and stiffness matrices. Finally, knowing the six polynomial solutions, it is possible—for any set of applied loads—to recover the 3D stress and strain states, either in the global or in the material reference frame.

2.6. Postprocessing

A powerful feature of SONATA consists of the results evaluation and plotting functionalities. By using the CAD-Kernel OpenCascade pythonOCC, lofted 3D geometries and 2D meshes can be generated and extracted. The cross-sectional outputs include the Timoshenko stiffness matrix, inertia matrix, center of mass, elastic center, and shear center, as well as the stress, strain, and displacement vectors of each finite element. Plotting functionalities address those outputs on a 2D and 3D level. Besides directly evaluating the results through extraction and plotting of results, the resulting 1D structural properties can be directly coupled to aeroelastic analysis models. Such coupling can be wrapped in an OpenMDAO [44] framework to conduct structural blade design optimization.

3. Box beam numerical analysis

Only a few known means of validation exist for the theory behind anisotropic beams. Stiffness results can be compared using results from 3D finite element models that have a very high degree of accuracy and potentially millions of degrees of freedom, or precisely conducted experiments that are detailed enough to also account for the small terms. Such validation is beyond the scope of this work and should be accounted for in future research. In the following, results from SONATA, using both VABS and ANBA4, are compared to other well-investigated approaches from literature based on VABS and NABSA data for the very same test cases. Current verification objectives are to demonstrate the accuracy of the parametric processing, topology, and meshing features within SONATA, and its interfaces to VABS and ANBA4. While VABS is a commercial off-the-shelf solution, the following comparisons of ANBA4 results with both current VABS results and previous studies from literature serve to gain confidence in using the current version of ANBA4 as a valuable open-source option. All the examples make use of linear triangular elements.

Table 1
Box beam geometrical properties.

Description	Parameter	Value, m
Width	a	0.0242
Height	b	0.0136
Length	L	0.764
Ply thickness	t_{ply}	1.27 E-04
Wall thickness (6 plies)	t	7.62 E-04

Table 2
AS4/3501-6 graphite/epoxy composite material properties.

Parameter	Property
E_l	142.0 GPa
E_t	9.79 GPa
G_{lt}	6.0 GPa
G_{tn}	4.8 GPa
ν_{lt}	0.42
ν_{tn}	0.34

Consider a composite box beam in three different CUS layup configurations, $[0^\circ]_6$, $[-15^\circ]_6$, and $[-30^\circ, 0^\circ]_3$. The fiber-orientation angles denoted in this work are in accordance with the coordinate system shown in Fig. 5. Box beam geometry properties are shown in Table 1 and material properties in Table 2. In terms of the material properties, layup $[-15^\circ]_6$ has a different Poisson's ratio of $\nu_{lt} = 0.3$. The order of the given stiffness is: 1 – extension; 2, 3 – shear; 4 – torsion; and 5, 6 – bending. The box beams (see Fig. 10) were analyzed using 200 equidistant points along the outer shape, resulting in a total of 1,481 nodes and 2,536 mesh elements.

Eq. (7) shows the relations between the Timoshenko stiffness matrix, S, resulting strains, ε, as well as elastic twist and curvatures, κ, when being loaded to sectional forces, F, and moments, M. The individual S_{ij} components follow the L-coordinate system conventions; see Fig. 3.

$$\begin{pmatrix} F_1 \\ F_2 \\ F_3 \\ M_1 \\ M_2 \\ M_3 \end{pmatrix} = \begin{bmatrix} S_{11} & S_{12} & S_{13} & S_{14} & S_{15} & S_{16} \\ S_{12} & S_{22} & S_{23} & S_{24} & S_{25} & S_{26} \\ S_{13} & S_{23} & S_{33} & S_{34} & S_{35} & S_{36} \\ S_{14} & S_{24} & S_{34} & S_{44} & S_{45} & S_{46} \\ S_{15} & S_{25} & S_{35} & S_{45} & S_{55} & S_{56} \\ S_{16} & S_{26} & S_{36} & S_{46} & S_{56} & S_{66} \end{bmatrix} \cdot \begin{pmatrix} \varepsilon_1 \\ \varepsilon_2 \\ \varepsilon_3 \\ \kappa_1 \\ \kappa_2 \\ \kappa_3 \end{pmatrix} = S \cdot \begin{pmatrix} \varepsilon_1 \\ \varepsilon_2 \\ \varepsilon_3 \\ \kappa_1 \\ \kappa_2 \\ \kappa_3 \end{pmatrix} \tag{7}$$

Table 3 shows the results with a $[0^\circ]_6$ layup. Off-diagonal terms were negligible for this simple example. The first two columns show literature [22] results using NABSA and VABS, while the latter two

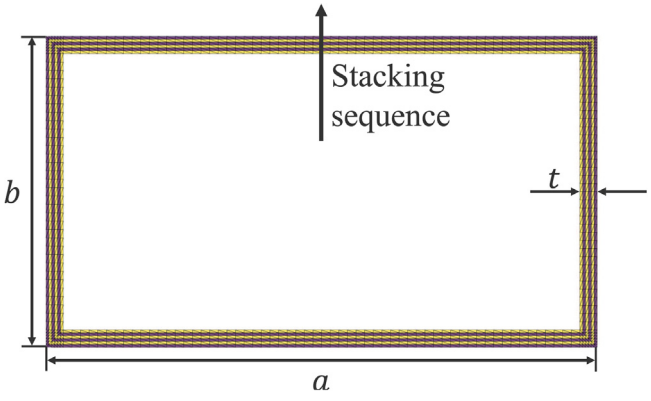

Fig. 10. Box beam cross-sectional geometry, topology, and discretized mesh.

Table 3
Stiffness of a prismatic box beam with a $[0^\circ]_6$ layup.

Stiffness	NABSA [22]	VABS [22]	SONATA/VABS	SONATA/ANBA4
S_{11}, N	7.8765 E+06	7.8765 E+06	7.8603 E+06	7.8603 E+06
S_{22}, N	1.9758 E+05	1.9803 E+05	1.9764 E+05	1.9764 E+05
S_{33}, N	8.4550 E+04	8.4995 E+04	8.4745 E+04	8.4745 E+04
S_{44}, Nm^2	2.3400 E+01	2.3500 E+01	2.3471 E+01	2.3471 E+01
S_{55}, Nm^2	2.4900 E+02	2.4900 E+02	2.4951 E+08	2.4951 E+02
S_{66}, Nm^2	6.1700 E+02	6.1700 E+02	6.1619 E+08	6.1619 E+02

Table 4
Stiffness of a Prismatic Box Beam with a $[-15^\circ]_6$ Layup

Stiffness	NABSA [57,14]	VABS [14]	SONATA/VABS	SONATA/ANBA4
S_{11}, N	6.3947 E+06	6.3947 E+06	6.3636 E+06	6.3636 E+06
S_{14}, Nm	1.2139 E+04	1.2139 E+04	1.2030 E+04	1.2030 E+04
S_{22}, N	4.0157 E+05	4.0170 E+05	3.9458 E+05	3.9458 E+05
S_{25}, Nm	−5.8787 E+03	−5.8787 E+03	−5.8417 E+03	−5.8417 E+03
S_{33}, N	1.7533 E+05	1.7546 E+05	1.7543 E+05	1.7543 E+05
S_{36}, Nm	−6.3692 E+03	−6.3692 E+03	−6.3106 E+03	−6.3106 E+03
S_{44}, Nm^2	4.8200 E+01	4.8200 E+01	4.8412 E+01	4.8412 E+01
S_{55}, Nm^2	1.9000 E+02	1.9000 E+02	1.9426 E+02	1.9426 E+02
S_{66}, Nm^2	4.9500 E+02	4.9500 E+02	4.9453 E+02	4.9453 E+02

Table 5
Stiffness of a Prismatic Box Beam with a $[-30^\circ, 0^\circ]_3$ Layup

Stiffness	NABSA [22]	SONATA/VABS	SONATA/ANBA4
S_{11}, N	5.5625 E+06	5.5400 E+06	5.5400 E+06
S_{14}, Nm	5.8889 E+03	5.8832 E+03	5.8832 E+03
S_{22}, N	4.3655 E+05	4.3695 E+05	4.3695 E+05
S_{25}, Nm	−2.9840 E+03	−2.9803 E+03	−2.9803 E+03
S_{33}, N	1.8868 E+05	1.8898 E+05	1.8898 E+05
S_{36}, Nm	−3.1422 E+03	−3.1432 E+03	−3.1432 E+03
S_{44}, Nm^2	5.0800 E+01	5.0867 E+01	5.0867 E+01
S_{55}, Nm^2	1.7600 E+02	1.7622 E+02	1.7622 E+02
S_{66}, Nm^2	4.3600 E+02	4.3584 E+02	4.3584 E+02

columns show the results from SONATA, using either VABS or ANBA4 as a structural solver. Table 3 shows that the stiffness values derived through SONATA between VABS and ANBA4 are identical, and the comparison of those to NABSA and VABS from previous work successfully verifies the accuracy of the SONATA framework. Minor differences were insignificant and can at least in part be attributed to the parametric topology and mesh generation in SONATA. One interesting finding was that the SONATA results between VABS and ANBA4 are identical, and minor differences can be seen between NABSA and VABS from literature. However, it eludes the authors' knowledge about potential meshing or other differences between those data from literature.

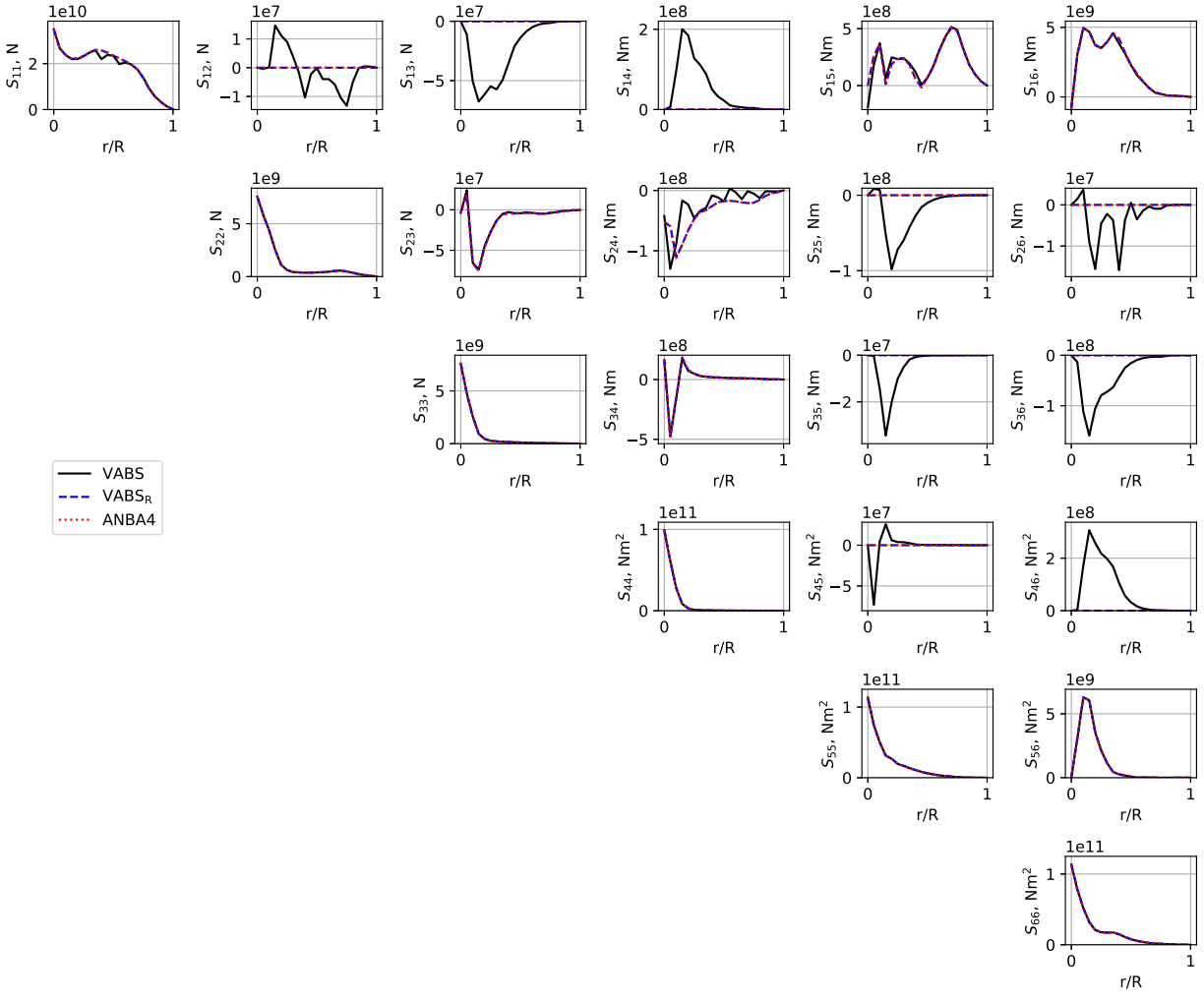

Fig. 11. Timoshenko stiffness matrix verification between VABS, VABS$_R$ (excludes effects from initial twist and curvature), and ANBA4 along the nondimensional blade span, r/R, for the 15-MW reference wind turbine blade.

Table 4 shows results with all plies being identically oriented in a $[-15^\circ]_6$ layup and Table 5 in a $[-30^\circ, 0^\circ]_3$ layup. Both examples result in additional extension–torsion, S_{14}, and shear-bending, S_{25} and S_{36}, coupling terms. The SONATA/VABS and SONATA/ANBA4 results were again identical and both showed excellent agreement with the literature. Even though VABS results from literature for the $[-30^\circ, 0^\circ]_3$ layup are available [22], they were excluded for this work because they were computed using an older version of VABS. Since VABS version 3.2, the energy transformation equations into the generalized Timoshenko stiffness matrix were redefined, thereby solving two previous inconsistencies that impacted the predicted generalized Timoshenko stiffness matrix. Those changes can measurably impact stiffness results, such as in a box beam layup with nonzero material orientation angles. This was explained in detail by Ho et al. [55].

4. Wind turbine blade analysis

This section analyzes the recently published 15-MW reference wind turbine blade [56]. The example demonstrates the capabilities of SONATA and was appraised suitably to further verify the usage of ANBA4 in comparison to VABS. The blade is 117 m long and has a root diameter of 5.2 m, a maximum chord of 5.77 m at $r/R = 0.272$, and a mass of approximately 65 tons. The blade 3D geometry and six exemplary cross sections were previously illustrated in Fig. 1. Its internal structure consists of unidirectional and triaxial glass-composite materials, carbon-composite spar caps, and additional layers of foam and gelcoat. Fig. 11 shows the fully resolved symmetrical Timoshenko stiffness matrix of the blade structural characteristics. Fig. 12 furthermore presents the inertia properties, including the section mass, μ, the mass moment of inertia, i_{22}, about the x_2 axis, the mass moment of inertia, i_{33}, about the x_3 axis, and the product of inertia, i_{23}, as well as the mass center, x_m, the tension center, x_t, and the shear center, x_s, locations. Results were computed at 21 equidistant radial station cross sections. The shear center, or so-called elastic axis, is the point in a cross section where the application of loads does not cause elastic twisting, and the tension center, or so-called neutral axis, is the point in a cross section that encounters zero longitudinal stresses or strains (i.e., zero axial force) when being applied with bending moments.

VABS_R data represent the reduced form of the VABS results, neglecting effects from initial twist and curvature. Hence, it accounts for the same features and is, therefore, well suited for a code-to-code comparison with ANBA4. Within the assumption of neglecting initial twist and curvature, results in Figs. 11 and 12 show that—besides being verified through box beam examples (see Section 3)—the verification of ANBA4 was again successful when applied to a fully resolved wind turbine blade. ANBA4 can, therefore, be seen as an applicable and open-source solver within SONATA for the analysis of slender composite structures such as blades.

The wind turbine blade incorporates axial-bend, S_{15} and S_{16}, and bend-bend, S_{56}, coupling terms. Because of the plies being entirely oriented in an axial direction, bend-twist coupling (S_{45} and S_{46}) originates solely from initial twist and curvature; see VABS results in Fig. 11.

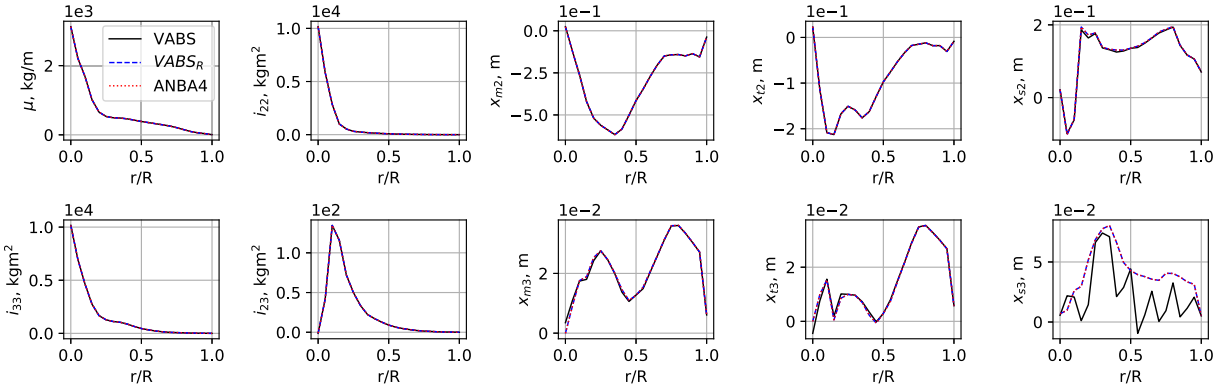

Fig. 12. Verification of inertia-matrix properties and axes locations between VABS, VABS_R (excludes effects from initial twist and curvature), and ANBA4 along the nondimensional blade span, r/R, for the 15-MW reference wind-turbine blade.

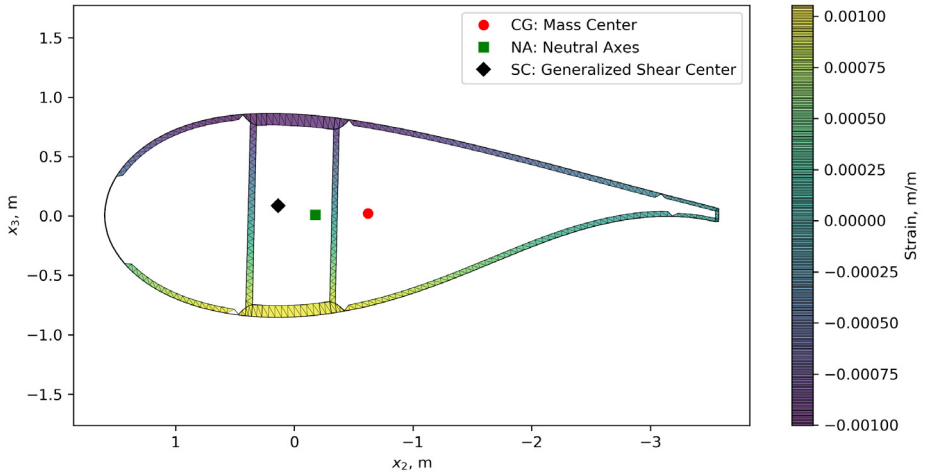

Fig. 13. Recovered strains in material-fiber direction at r/R = 0.325 of the wind turbine blade. Applied cross-sectional loads were determined through coupling with BeamDyn.

SONATA determines the initial state inputs automatically, based on the outer geometry of the blade. Note that this feature is yet to be added for ANBA4. Small discontinuities in the VABS results (e.g., S_{24} or x_{s3}) are based on the initial twist and curvature states in a cross section and may, at least in part, originate from slightly inaccurate outer shape definitions of the blade model. The shear-center location is a function of the shear-torsion coupling terms, $x_{s2} = f(S_{34})$ and $x_{s3} = f(S_{24})$. Therefore, x_{s3} shows similar fluctuating characteristics as S_{24}. Detailed sensitivity studies and potential impacts from initial states on the blades' aeroelastic behavior will be investigated in future work.

Fig. 13 shows recovered strains (see also Eq. 7) of one blade cross section at about 1/3 span. The results shown were determined using ANBA4 but are identical with VABS. Applied cross-sectional loads were determined using BeamDyn within OpenFAST at an above-rated steady wind speed of 12 m/s, which incorporated the fully resolved mass and stiffness matrices (see Fig. 11) from SONATA. BeamDyn uses the geometrically exact beam theory [18] for 1D beams, based on the Legendre spectral finite element method. Resulting strains were dominated by flapwise moments. Conducting such recovery analysis results in stresses, strains, and deformations in any direction. Those are important to analyze and optimize blades based on material safety constraints. Fig. 13 furthermore shows the resulting mass center, neutral axes, and shear center that were again successfully verified between VABS and ANBA4; see Fig. 12.

5. Conclusions

This work presents the methodology of SONATA, an efficient parametric design framework to investigate slender composite structures. SONATA's parametrization, cross-sectional topology generation, and mesh discretization approaches, as well as the structural solvers (VABS and ANBA4) for determining the stiffness characteristics are presented and verified. The tool features coupling to aeroelastic analysis and enables structural composite-blade design analysis and optimization. The following specific conclusions can be drawn:

- Using ANBA4 instead of VABS extends the SONATA framework to being a fully open-source available cross-sectional structural analysis and optimization environment that can be applied to either rotorcraft, wind turbine blades, or other slender composite structures of arbitrary cross sections.
- SONATA's parametric preprocessing, topology generation, mesh discretization, and solver integration of both VABS and ANBA4 were successfully verified through a comparison with literature results of composite box beams derived through VABS and NABSA.
- Embedded in SONATA, both VABS and ANBA4 proved to be well suited to analyze complex slender composite structures, such as modern large and highly flexible wind turbine blades, including stress and strain recovery as well as bend-twist coupling effects.
- The SONATA framework effectively enables 3D blade design in connection with 1D beam finite element models. This allows a tight connection between aeroelastic analysis simulation and the blade-structural design, thereby offering a systematic development process for high-fidelity and multidisciplinary blade optimization.
- To enhance the confidence of modern rotorcraft or wind turbine blade designs and better address cost and safety requirements, SONATA allows to incorporate material failure criteria, manufacturing constraints, and material and manufacturing uncertainties. Material failure criteria can be accounted for in the design process by recovering stresses and strains with strong connection to aeroelastic simulations.

The parametric modeling approach to investigate slender composite structures with a high-fidelity structural accuracy provides an effective analysis and optimization framework. It will further be used for multidisciplinary blade optimization tasks with both helicopter and wind turbine blade applications to account for the entire rotor system with respect to target objectives such as performance, mean and vibratory loads, blade deflections, aeroelastic stability, and structural integrity. Future work will extend ANBA4 to also account for initial twist and curvature effects, and further verification studies will include comparisons to 3D finite element models.

6. Data availability

The raw/processed data, i.e. the SONATA git repository, including examples required to reproduce these findings, are available at https://gitlab.lrz.de/HTMWTUM/SONATA.

Declaration of Competing Interest

The authors declare that they have no known competing financial interests or personal relationships that could have appeared to influence the work reported in this paper.

Acknowledgements

This work was authored in part by the National Renewable Energy Laboratory, operated by Alliance for Sustainable Energy, LLC, for the U.S. Department of Energy (DOE) under Contract No. DE-AC36-08GO28308. Funding was provided by the U.S. Department of Energy Office of Energy Efficiency and Renewable Energy Wind Energy Technologies Office. The views expressed herein do not necessarily represent the views of the DOE or the U.S. Government. The U.S. Government retains and the publisher, by accepting the article for publication, acknowledges that the U.S. Government retains a nonexclusive, paid-up, irrevocable, worldwide license to publish or reproduce the published form of this work, or allow others to do so, for U.S. Government purposes.

In addition, the work from the Technical University of Munich was funded by the German Federal Ministry for Economic Affairs and Energy through the German Aviation Research Program LuFo V-2 within the project VARI-SPEED.

References

[1] Adelman HM, Mantay WR. Integrated multidisciplinary optimization of rotorcraft: A plan for development. Tech. rep. NASA Langley Research Center 1989: TM–101617.
[2] Rohl P.J., Kumar D., Dorman P., Sutton M., Cesnik C.E.S., A composite rotor blade structural design environment for aeromechanical assessments in conceptual and preliminary design. In: American helicopter society 68th annual forum. American Helicopter Society, Fort Worth, TX, May 1–3, 2012.
[3] Johnson W. A history of rotorcraft comprehensive analyses. In: American helicopter society 60th annual forum, Baltimore, MD, June 7–10, 2013.
[4] Bauchau OA, Bottasso C, Nikishkov Y. Modeling rotorcraft dynamics with finite element multi-body procedures. J Math Comput Model 2001;33(10–11):1113–37. https://doi.org/10.1016/S0895-7177(00)00303-4.
[5] Masarati P, Morandini M, Mantegazza P. An efficient formulation for general-purpose multibody/multiphysics analysis. J Comput Nonlinear Dyn 2014;9(4). https://doi.org/10.1115/1.4025628. 041001.
[6] Wang Q, Sprague MA, Jonkman JM, Johnson N, Jonkman B. BeamDyn: a high-fidelity wind turbine blade solver in the FAST modular framework. J Wind Energy 2017;20(8):1–24. https://doi.org/10.1002/we.2101.
[7] Jonkman JM, Buhl Jr ML. FAST User's Guide. National Renewable Energy Laboratory 2005.
[8] Sprague M.A., Jonkman J.M., Jonkman B.J. FAST modular framework for wind turbine simulation: New algorithms and numerical examples. In: AIAA SciTech, 33rd wind energy symposium, Kissimmee, FL, January 5–9, 2015.
[9] Datta A, Johnson W. Three-dimensional finite element formulation and scalable domain decomposition for high-fidelity rotor dynamic analysis. J Am Helicopt Soc 2011;56(2):22003. https://doi.org/10.4050/JAHS.56.022003.
[10] Yeo H., Truong K., Ormiston R.A. Assessment of 1-D versus 3-D methods for modeling rotor blade structural dynamics. In: 51st AIAA/ASME/ASCE/AHS/ASC structures, structural dynamics, and materials conference, Orlando, FL, April 12–15, 2010. doi:10.2514/6.2010-3044.

[11] Rohl P., Dorman P., Sutton M., Kumar D., Cesnik C.E.S. A multidisciplinary design environment for composite rotor blades. In: 53rd AIAA/ASME/ASCE/AHS/ASC structures, structural dynamics and materials conference, Honolulu, HI, April 23–26, 2012, pp. 1–15.

[12] Li L. Structural design of composite rotor blades with consideration of manufacturability, durability, and manufacturing uncertainties. Ph.D. thesis, Georgia Institute of Technology; 2008.

[13] Giavotto V, Borri M, Mantegazza P, Ghiringhelli G, Carmaschi V, Maffioli G. Anisotropic beam theory and applications. J Comput Struct 1983;16(1–4):403–13. https://doi.org/10.1016/0045-7949(83)90179-7.

[14] Yu W, Hodges DH, Ho JC. Variational asymptotic beam sectional analysis – an updated version. J Eng Sci 2012;59:40–64. https://doi.org/10.1016/j.ijengsci.2012.03.006.

[15] Blasques JP. Multi-material topology optimization of laminated composite beams with eigenfrequency constraints. J Compos Struct 2014;111:44–55. https://doi.org/10.1016/j.compstruct.2013.12.021.

[16] Blasques JP, Stolpe M. Multi-material topology optimization of laminated composite beam cross sections. J Compos Struct 2012;94:3278–89. https://doi.org/10.1016/j.compstruct.2012.05.002.

[17] Cesnik C.E.S., Hodges D.H. VABS: A new concept for composite rotor blade cross-sectional modeling. In: American helicopter society 51st annual forum, Fort Worth, TX, May 9–11, 1995.

[18] Hodges DH. A mixed variational formulation based on exact intrinsic equations for dynamics of moving beams. J Solids Struct 1990;26(11):1253–73. https://doi.org/10.1016/0020-7683(90)90060-9.

[19] Berdichevsky VL. Variational-asymptotic method of constructing a theory of shells. J Appl Math Mech 1979;43(4):664–87. https://doi.org/10.1016/0021-8928(79)90157-6.

[20] Hodges DH. Geometrically Exact, Intrinsic Theory for Dynamics of Curved and Twisted Anisotropic Beams. AIAA J 2003;41(6). https://doi.org/10.2514/2.2054.

[21] Yu W. Vabs manual for users, Tech. rep., Utah State University Technology Commercialization Office and Georgia Institute of Technology Research Cooperation; 2011.

[22] Popescu P, Hodges DH. On asymptotically correct Timoshenko-like anisotropic beam theory. J Solids Struct 2000;37:535–58. https://doi.org/10.1016/S0020-7683(99)00020-7.

[23] Cesnik C.E.S., Mok J., Parikh A., Shin S. Optimum design framework for integrally twisted helicopter blades. In: 45th AIAA/ASME/ASCE/AHS/ASC structures, structural dynamics and materials conference, Palm Springs, CA, April 19–22, 2004. doi:10.2514/6.2004-1761.

[24] Feil R. Aeromechanics analysis of counter-rotating coaxial rotor systems. Ph.D. thesis, Technical University of Munich; 2019. ISBN 978-3-8439-4086-3.

[25] Morandini M, Chierichetti M, Mantegazza P. Characteristic behavior of prismatic anisotropic beam via generalized eigenvectors. Int J Solids Struct 2010;47(10):1327–37. https://doi.org/10.1016/j.ijsolstr.2010.01.017.

[26] Han S, Bauchau OA. On saint-venant's problem for helicoidal beams. J Appl Mech 2015;83(2). https://doi.org/10.1115/1.4031935.

[27] Heath CM, Gray JS. OpenMDAO: Framework for flexible multidisciplinary design, analysis and optimization methods. AIAA J 2013;51:2380–94. https://doi.org/10.2514/6.2012-1673.

[28] Silva C, Johnson W. Multidisciplinary conceptual design for reduced-emission rotorcraft. In: AHS specialists conference on aeromechanics design for transformative vertical flight, AHS, San Francisco, CA, January 16–18, 2018.

[29] Li L. Structural design of composite rotor blades with consideration of manufacturability, durability, and manufacturing uncertainties. Ph.D. thesis, Georgia Institute of Technology; 2008.

[30] Ghiringhelli GL, Masarati P, Morandini M, Muffo D. Integrated aeroservoelastic analysis of induced strain rotor blades. Mech Adv Mater Struct 2008;15(3–4):291–306. https://doi.org/10.1080/15376490801907822.

[31] Lim J, Shin S, Kee Y. Optimization of rotor structural design in compound rotorcraft with lift offset. J Am Helicopt Soc 2016;61(1):1–14. https://doi.org/10.4050/JAHS.61.012005.

[32] Kumar D, Cesnik C.E.S. Optimization framework for the dynamic analysis and design of active twist rotors. In: American helicopter society 68th annual forum, Forth Worth, TX, May 1–3, 2012.

[33] Kumar D, Cesnik CES. New optimization strategy for design of active twist rotors. AIAA J 2015;53(2):436–48. https://doi.org/10.2514/1.J053195.

[34] Meyn L.L. Rotorcraft optimization tools: Incorporating design codes into multi-disciplinary design, analysis and optimization. In: AHS specialists meeting on aeromechanics design for transformative vertical lift, San Francisco, CA, January 16–18, 2018.

[35] Glaz B., Friedmann P.P., Liu L., Kumar D., Cesnik C.E.S. The AVINOR aeroelastic simulation code and its application to reduced vibration composite rotor blade design. In: 50th AIAA/ASME/ASCE/AHS/ASC structures, structural dynamics, and materials conference, Palm Springs, CA, 4–7 May, 2009. doi:10.2514/6.2009-2601.

[36] Glaz B, Friedmann PP, Liu L. Helicopter vibration reduction throughout the entire flight envelope using surrogate-based optimization. J Am Helicopt Soc 2009;54(1):12007. https://doi.org/10.4050/JAHS.54.012007.

[37] Hui C, Yu W, Capellaro M. A critical assessment of computer tools for calculating composite wind turbine blade properties. J Wind Energy 2009;13(6):497–516. https://doi.org/10.1002/we.372.

[38] Bir G. Computerized method for preliminary structural design of composite wind turbine blades. J Solar Energy Eng 2001;124(4):372–81. https://doi.org/10.1115/1.1413217.

[39] Philippidis T, Vassilopoulos A, Katopis K, Voutsinas S. THIN/PROBEAM: a software for fatigue design and analysis of composite rotor blades. J Wind Eng 1996;20(5):349–62. https://www.jstor.org/stable/43749625.

[40] Lindenburg C. STABLAD-stability analysis tool for anisotropic rotor blade panels. Tech. Rep. ECN-CX-99-031, Energy Research Center of the Netherlands 2008.

[41] Friedmann PP. Helicopter vibration reduction using structural optimization with aeroelastic/multidisciplinary constraints – a survey. J Aircraft 1990;28(1):8–21. https://doi.org/10.2514/3.45987.

[42] Weller W.H., Davis M.W. Wind tunnel tests of helicopter blade designs optimized for minimum vibration. In: American helicopter society 44th annual forum, Washington, D.C., June 16–18, 1988..

[43] Paviot T. pythonocc, 3D CAD/CAE/PLM development framework for the Python programming language, PythonOCC – 3D CAD Python. http://www.pythonocc.org/ (accessed April 24, 2020).

[44] Gray JS, Hwang JT, Martins JR, Moore KT, Naylor BA. OpenMDAO: An open-source framework for multidisciplinary design, analysis, and optimization. J Struct Multidisip Opt 2019;59(4):1075–104. https://doi.org/10.1007/s00158-019-02211-z.

[45] Pflumm T, Garre W, Hajek M. A preprocessor for parametric composite rotor blade cross-sections 2018;18–21 September.

[46] Pflumm T., Garre W., Hajek M. Propagation of material and manufacturing uncertainties in composite helicopter rotor blades. In: 45th European rotorcraft forum, Warsaw, Poland, September 17–20, 2019.

[47] Shewchuk JR. Triangle: Engineering a 2D quality mesh generator and delaunay triangulator. In: Lin MC, Manocha D, editors. Applied computational geometry: towards geometric engineering, vol. 1148. Springer-Verlag; 1996. p. 203–22.

[48] Hodges DH. Nonlinear composite beam theory for engineers. AIAA; 2006.

[49] Zhu W, Morandini M. Multiphysics cross-section analysis of smart beams. Mech Adv Mater Struct 2020:1–18. https://doi.org/10.1080/15376494.2020.1731886.

[50] Anba4, commit 28c0dbb, Accessed on May 11th, 2020 (May 2020). URL https://bitbucket.org/anba_code/anba_v4.

[51] Logg A, Wells GN. DOLFIN: Automated finite element computing. ACM Trans Math Softw 2010;37(2):1–28. https://doi.org/10.1145/1731022.1731030.

[52] Logg A, Wells GN, Hake J. DOLFIN: a C++/python finite element library. Springer; 2012. Ch. 10.

[53] Alnæs MS, Blechta J, Hake J, Johansson A, Kehlet B, Logg A, Richardson C, Ring J, Rognes ME, Wells GN. The FEniCS project version 1.5. Arch Numer Softw 2015;3(100):9–23. https://doi.org/10.11588/ans.2015.100.20553.

[54] Logg A, Mardal KA, Wells GN. Automated solution of differential equations by the finite element method. Springer 2012. https://doi.org/10.1007/978-3-642-23099-8.

[55] Ho J, Yu W, Hodges D. Energy transformation to generalized Timoshenko form by the variational asymptotic beam sectional analysis. In: 51st AIAA/ASME/ASCE/AHS/ASC structures, structural dynamics, and materials conference, Orlando, Florida, 2010. doi:10.2514/6.2010-3017.

[56] Gaertner E., Rinker J., Sethuraman L., Zahle F., Anderson B., Barter G., Abbas N., Meng F., Bortolotti P., Skrzypinski W., Scott G., Feil R., Bredmose H., Dykes K., Sheilds M., Allen C., Viselli A. Definition of the IEA 15 MW offshore reference wind turbine. Tech. Rep. NREL/TP-75698, International Energy Agency; 2020.

[57] Yu W, Hodges DH, Volovoi V, Cesnik C. On Timoshenko-like modeling of initially curved and twisted composite beams. J Solids Struct 2002;39:5101–21. https://doi.org/10.1016/S0020-7683(02)00399-2.